Supporting Information

For

Reactive Oxygen Species Regulation and Synergistic for Effective Water Purification through Fenton-like Catalysis on Single-Atom Cu-N Sites

Shiyu Zuo[1], Zeyu Guan[1], Fan Yang[2], Dongsheng Xia[3], Dongya Li[1,4]*

[1] School of Environmental Engineering, Wuhan Textile University, Wuhan, 430073, P.R. China.

[2] School of Mathematical and Physical Sciences, Wuhan Textile University, Wuhan, 430073, P.R. China.

[3] Engineering Research Center Clean Production of Textile Dyeing and Printing, Ministry of Education, Wuhan, 430073, P.R. China.

[4] State Key Laboratory of New Textile Materials and Advanced Processing Technologies, Wuhan Textile University, Wuhan 430200, P. R. China.

*Corresponding author.

E-mail address: dyli@wtu.edu.cn.

This Supporting Information includes

4 Text

25 Figures

6 Table

List of Text, Figures and Table

Text S1. Chemicals and materials.

Text S2. Methods.

Text S3. Experiment.

Text S4 Material characterization.

Text S5 Electrochemical analysis tests.

Text S6 Calculation methods.

Fig. S1. SEM of C.

Fig. S2. BET of C and Cu-SA.

Fig. S3. (a) HAADF-STEM of Cu-SA; EDS of (b) Cu, (c) C and (d) N.

Fig. S4. FT-IR of C and Cu-SA.

Fig. S5. XPS Cu 2p of Cu-SA.

Fig. S6. XPS C 1s of C and Cu-SA.

Fig. S7. EPR of C and Cu-SA.

Fig. S8. EIS of C and Cu-SA.

Fig. S9. CV of C and Cu-SA.

Fig. S10. Adsorption of BPA in Cu-SA.

Fig. S11. Degradation of BPA in different systems (Cu-SA, ZVI, ZVC, Fe^{2+}, Cu^+).

Fig. S12. Degradation of BPA in different systems (Cu-SA/H_2O_2, Cu-SA/PDS, Cu-SA/PMS and Fe^{2+}/H_2O_2).

Fig. S13. (a) Cyclic experiment of BPA degradation in Cu-SA/PMS; (b) XRD after Cu-SA reaction; (c) XPS after Cu-SA reaction; (d) Cu^{2+} leaching of Cu-SA.

Fig. S14. Influence of MeOH in Cu-SA/H_2O_2.

Fig. S15. Influence of MeOH and NaN_3 in Cu-SA/PDS.

Fig. S16. Influence of MeOH and NaN_3 in Cu-SA/PMS.

Fig. S17. Oxidant consumption in Cu-SA/H_2O_2, Cu-SA/PDS and Cu-SA/PMS.

Fig. S18. Calculated energy profiles for (a) H_2O_2, (b) PDS, (c) PMS dissociation.

Text S1. Chemicals and materials.

Deionized water was used for the experiments. Hydrogen peroxide (H_2O_2, 30%), Sodium persulfate (PDS, $Na_2S_2O_8$, 98%), Peroxymonosulfate (PMS, >47%), 5,5-dimethyl-1-pyrroline N-oxide (DMPO, 97%) and 2,2,6,6-tetramethyl-4-piperidinol (TEMP, 99%) were obtained from Aladdin Reagent Co. Ethanol (EtOH, 99%), tert-butanol (TBA, 99%), furfuryl alcohol (FFA, 98%), potassium iodide (KI, 99%), Sodium dihydrogen phosphate (NaH_2PO_4, 99%), sodium chloride (NaCl, 99%), sodium carbonate ($NaHCO_3$, 99%), sodium carbonate (Na_2CO_3, 99%), sodium sulfate (Na_2SO_4, 99%), humic acid (90%), iron(III) chloride hexahydrate ($H_{12}Cl_3FeO_6·H_2O$, 99%), copper(II) acetate monohydrate ($C_4H_6CuO_4·H_2O$, 99.0%) , Phenol (C_6H_6O, 99%), p-Hydroxybenzoic acid ($C_7H_6O_3$, 99%), Bisphenol A (BPA, 99%), o-Chlorophenol (ClC_6H_4OH, 99%) and 2-Hydroxyterephthalic acid ($C_8H_6O_5$, 98%) were obtained from Sinopharm Chemical Reagent Co., Ltd. (China).

Text S2. Methods.

The potassium citrate was heated to 800 °C for 1 h under nitrogen atmosphere, the black powder was acid washed, and the obtained sample was C (carrier).

Mix 60 mg C, 6.7 mmol α-D-glucose and 0.3 mmol $Cu(NO_3)_2·6H_2O$ in water. After being washed with water and dried, it was mixed with 300 mg of melamine, and then calcined in a N_2 atmosphere at 800 °C for 2 h to finally obtain Cu-SA. According to ICP analysis, the Cu loading is about 1.6 w%.

Text S3. Experiment.

The solution of catalyst, oxidant and pollutant is mixed with magnetic stirring to make it fully react. The pH value is controlled by adding 10 mmol/L phosphate buffer (PB). The experiment was repeated more than three times. Use high-performance liquid chromatography (Shimadzu LC-16) with a C18 column (150 mm × 4.6 mm, 5 μm) to analyze the BPA concentration.

Text S4 Material characterization.

JEM ARM200F, acceleration voltage 200kV; HAADF uses a half-convergence angle of

25mrad, and a collection angle of about 85-365mrad. The X-ray absorption spectra(XAS) including X-ray absorption near-edge structure(XANES)and extended X-ray absorption fine stucture (EXAFS) of the samples at Cu K-edge (7709eV were colleted at the Singapore Synchrotron Light Source(SSLS)center, where a pair of chanel-cut Si (111) crystals was used in the monochromator. The Cu K-edge XANES data were recorded in a transmission mode.Cu foil and Cu_2O were used as references. The storage ring was working at the energy of 2.5 GeV with anaverage electron curent of below 200mA. The acquired EXAFS data were extracted and procsed acording to thestandard procedures using te ATHENA module implemented in the FEFIT sofware packages. The k3-weighted Fourier transform (FT) of x(k) in R space was obtained over herange of 0-14.0 Å-1 by applying a Besse window finction. The specific surface area and pore size distribution of materials were determined on the basis of N_2 adsorption at 77 K using surface and pore analyzer (Nova 3000, Quantachrome, Boynton Beach, FL). The morphology was characterized with scanning electron microscope (SEM, S-3400 II, Hitachi, Japan), transmission electron microscopy (TEM, JEM-200CX, JEOL, Japan), and high resolution transmission electron microscope (HR-TEM, Tecnai G2 F20 S, FEI, U.S.A.). X-ray diffraction (XRD, X'TRA, ARL, Switzerland) was used to investigate the mineralogy of the catalysts with Cu Kα radiation. The functional groups were characterized by Fourier transform infrared spectroscopy (FTIR, Nicolet iS5, Thermo Scientific, U.S.A.). X-ray photoelectron spectroscopy (XPS, ESCALAB-2, Great Britain) with an Al Kα anode radiation as the excitation source was employed to detect the chemical states of different elements. All the binding energies were referenced to the C 1s peak at 284.8 eV. Zeta potential (ZP) of samples was measured with a Zeta voltmeter (Zeta-sizer Nano ZS90). The degradation intermediates were identified by Ultra Performance Liquid Chromatography-mass spectrometry (UPLC-MS, Waters Xevo TQ-S, USA) with BEH-C18 (100 mm × 2.1 mm, 5 mm) column. Radicals ($SO_4^{\bullet-}$ and •OH) and singlet oxygen ($^1O_2$) were detected by employing electron paramagnetic resonance (EPR, EMX-10/12, Bruker, Germany) spectroscopy with DMPO and TEMP as the spin-trapping agent, respectively.

Text S5 Electrochemical analysis tests.

The FTO loaded with powder was first prepared. Nafion® solution (5.0 wt%, 0.01 mL) and catalyst (5 mg) were mixed with ethanol (0.1 mL), then ultrasonic dispersion for 3 h to form a

suspension solution. Next, 60 μL suspension was dropped onto the surface of the FTO electrode. The electrode was vacuum dried at 60 °C for 8 h. Silver/silver chloride electrode (Ag/AgCl) and Pt wire electrode were used as reference electrode and counter electrode, respectively. Electrochemical impedance spectroscopy (EIS) was carried out at open potential in 0.5 M Na_2SO_4 solution, and the frequency was in the range from 10^5 to 10^{-1} Hz. Linear sweep voltammetry (LSV) was measured at the potential from 0.0-1.5 V (vs. Ag/AgCl) with a scanning rate of 50 mV/s. Chronoamperometries were carried out at the bias of 0.0 V (vs. Ag/AgCl) with 0.5 M Na_2SO_4 as supporting electrolyte.

Text S6 Calculation methods.

We used the Vienna Ab initio simulation package (VASP) [1] based on self-consistent density functional theory [2, 3] to calculate the structure and electronic structure. The frozen-core projector augmented wave approach [4, 5] was employed to describe the core-valence interaction. The generalized gradient approximation [6], in the form proposed by Perdew, Burke, and Ernzerhof [7], was used for the exchange-correlation functional. For all calculations, the electronic states were expanded using a plane-wave basis set with a kinetic energy cutoff of 400 eV. For structural optimization, periodic boundary conditions were applied. The SACs structure was constructed in this way as follow steps: firstly, a $6 \times 6 \times 1$ supercell of graphene with double C atoms vacancy was used as surface models. And then, a single Cu atom embedded on hollow site on graphene, and it's nearest 4 carbon atoms were replaced by 4 nitrogen atoms. The calculated bond lengths are d_{Cu-N}=1.92 Å, d_{C-N1}=1.36 Å and d_{C-N2}=1.37 Å. We separated the surface by a vacuum of 18 Å to meet the needs of constructing the adsorbed system structures. k-point meshes were performed a $3 \times 3 \times 1$ Monkhorst-Pack with Γ–centered method for all calculations. Geometry relaxation were considered to converge when the force on each atom was less than 0.02 eV/Å and the energy tolerance was set as 1.0×10^{-5} eV/atom to ensure accurate results. DFT-D3 correction method of Grimme was used for non-local van der Waals (vdW) interactions[8]. The energy barriers for H_2O_2, PMS, PDS splitting on surfaces were calculated with climbing-image nudged elastic band (CI-NEB) method [9]. Structures of transition states were confirmed by vibrational frequency calculations.

A Gaussian 09 system was employed to optimized the BPA and Single-point energies were

calculated at the B3LYP/ 6-311G** level [10, 11]. The HOMO and LUMO was plotted using Multiwfn.
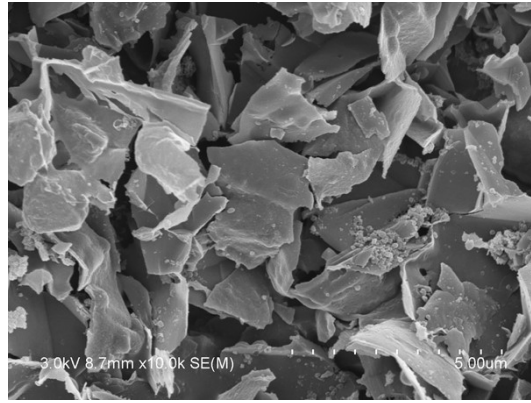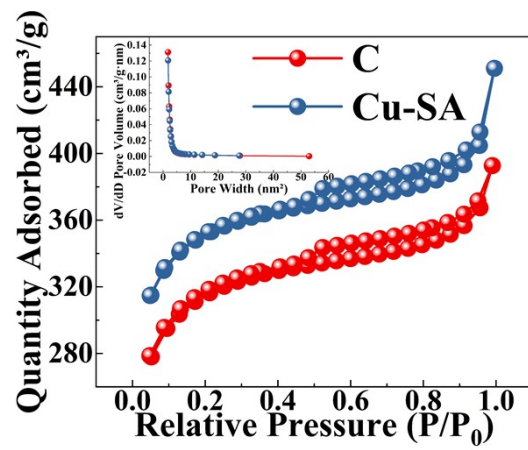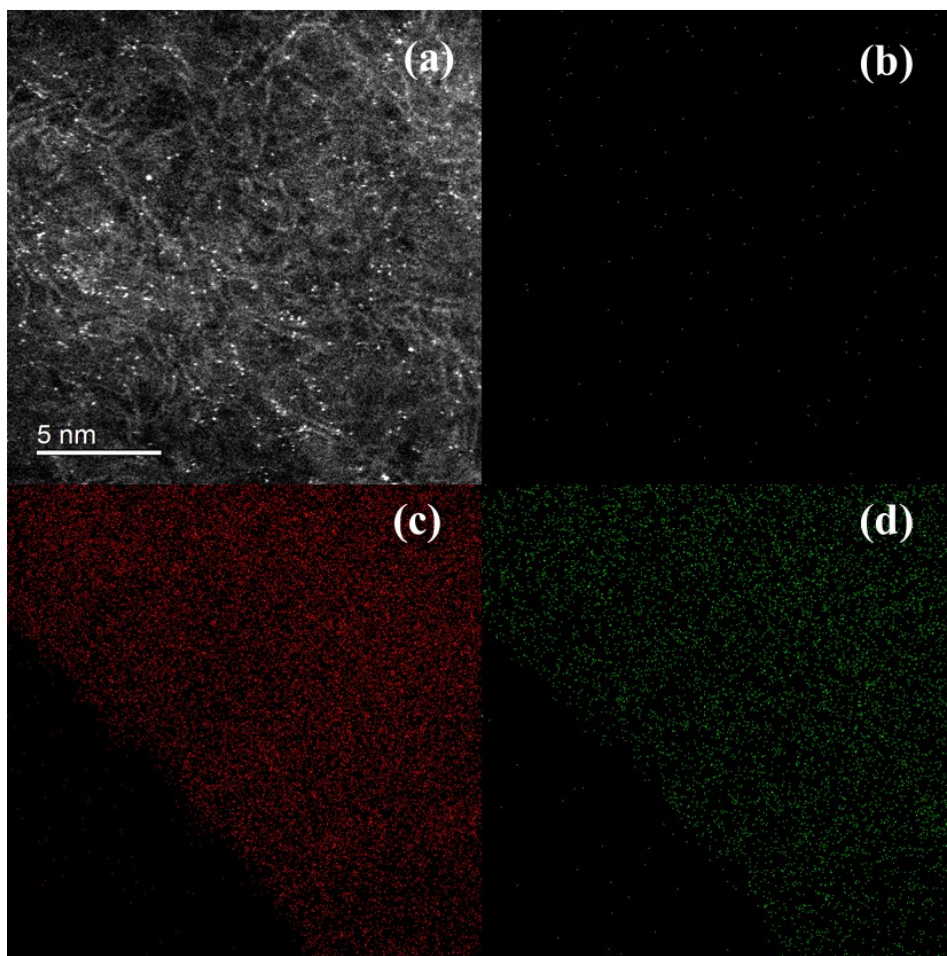
Fig. S1. SEM of C.

Fig. S2. BET of C and Cu-SA.

Fig. S3. (a) HAADF-STEM of Cu-SA; EDS of (b) Cu, (c) C and (d) N.
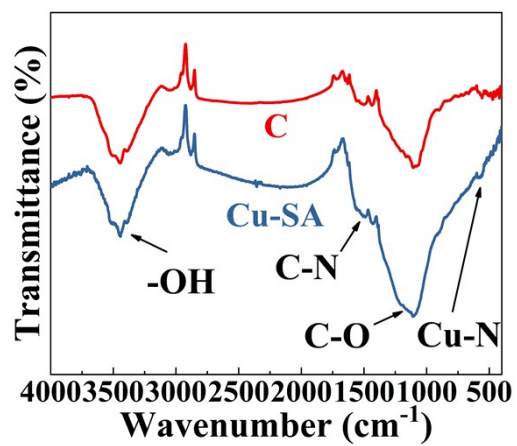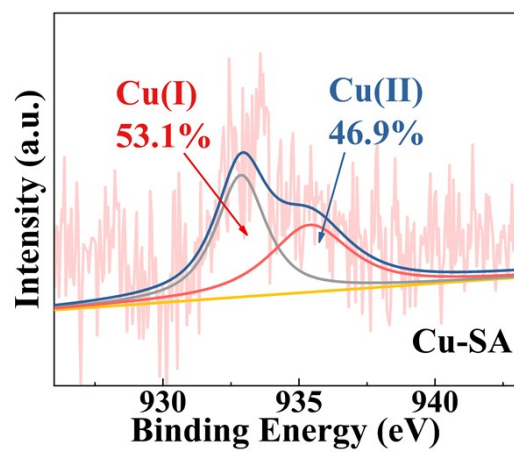
Fig. S4. FT-IR of C and Cu-SA.
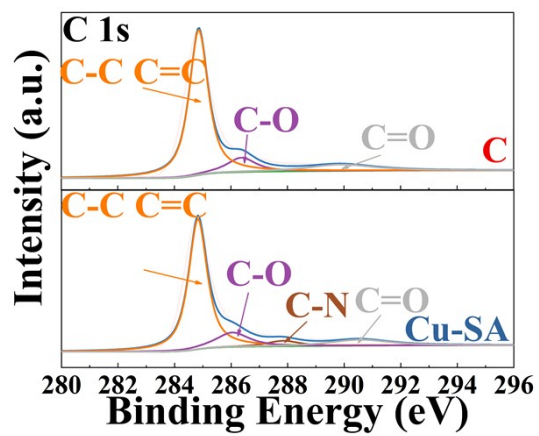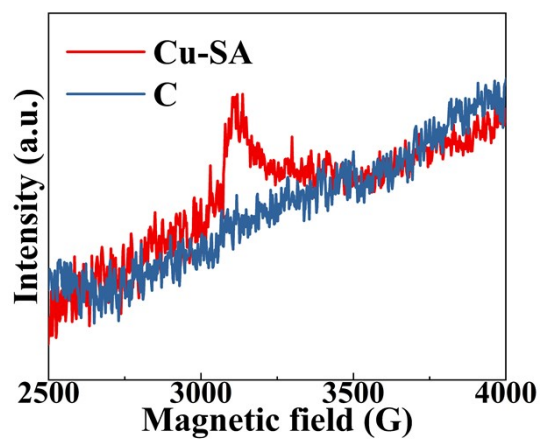
Fig. S5. XPS Cu 2p of Cu-SA.

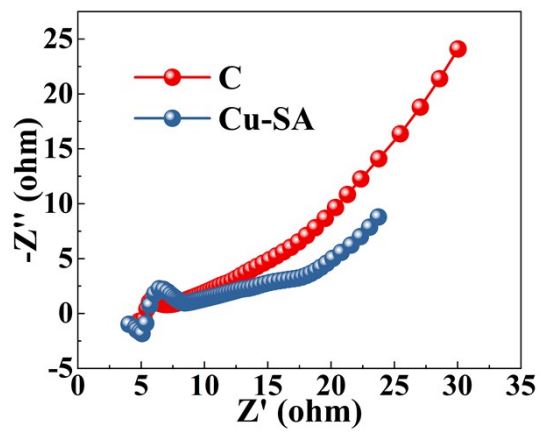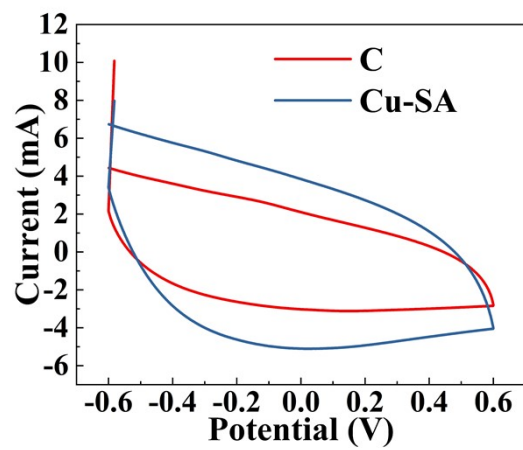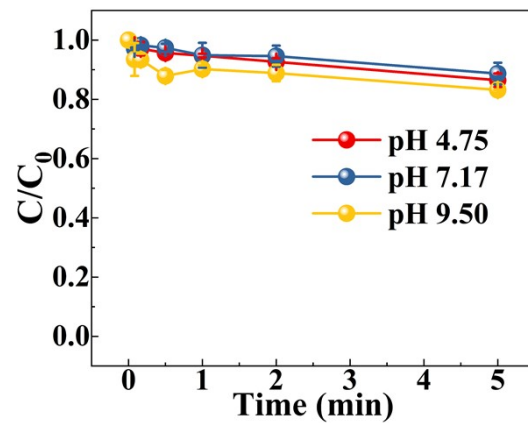**Fig. S6.** XPS C 1s of C and Cu-SA.

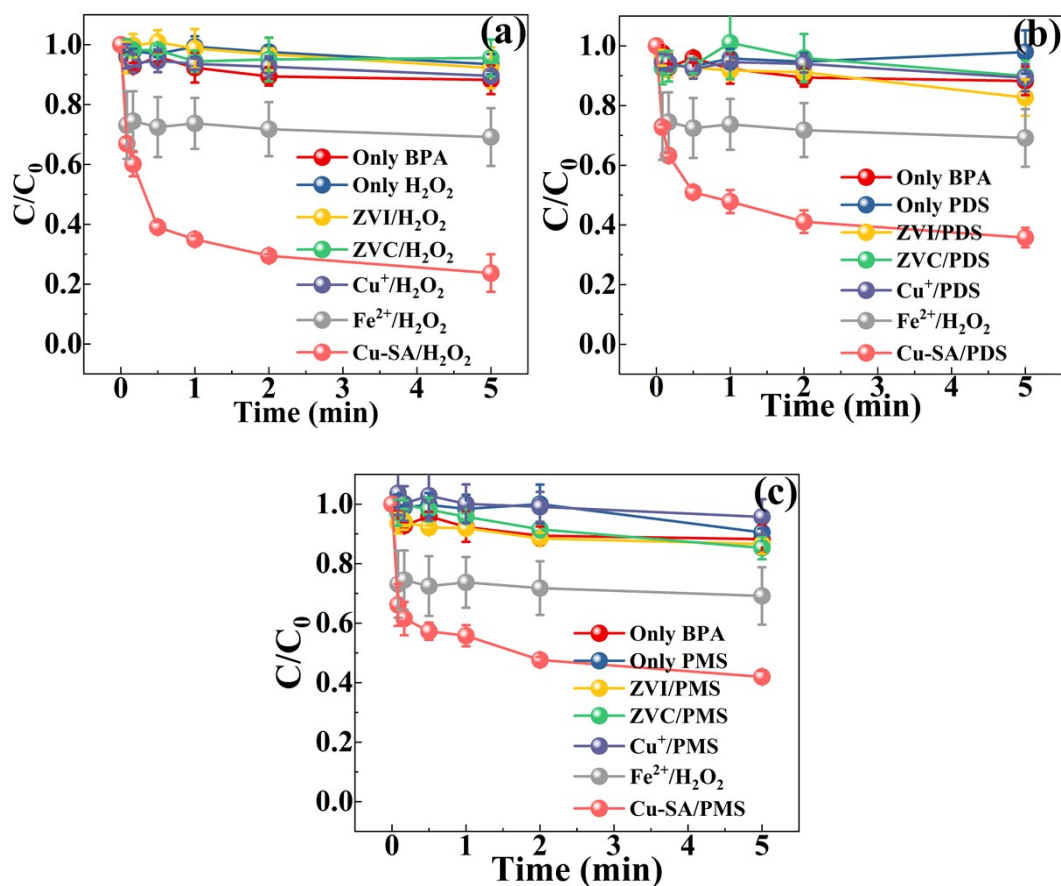**Fig. S7.** EPR of C and Cu-SA.

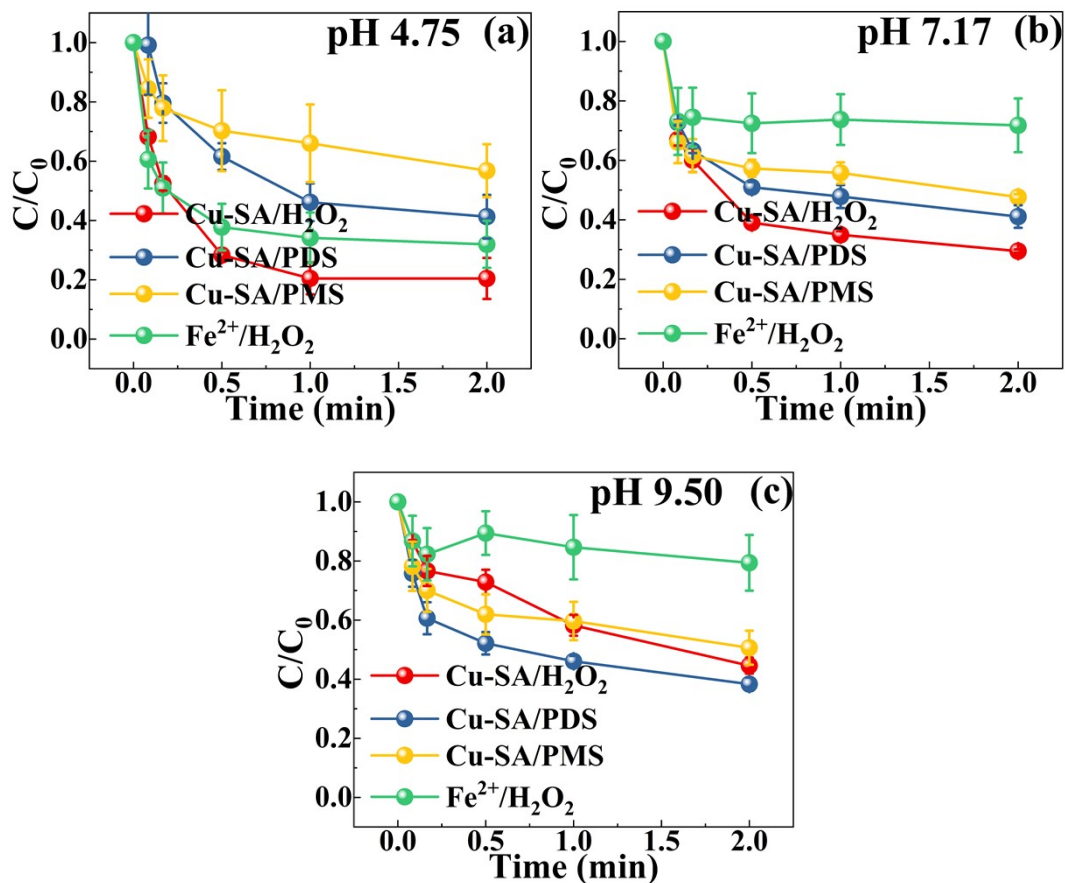**Fig. S8.** EIS of C and Cu-SA.

Fig. S9. CV of C and Cu-SA.

Fig. S10. Adsorption of BPA in Cu-SA.

[Catalyst]$_0$ = 0.1 g/L, [BPA]$_0$ = 0.1 mmol/L, [PB]$_0$ = 10 mmol/L and T = 278 K.

Fig. S11. Degradation of BPA in different systems (Cu-SA, ZVI, ZVC, Fe^{2+}, Cu^+).

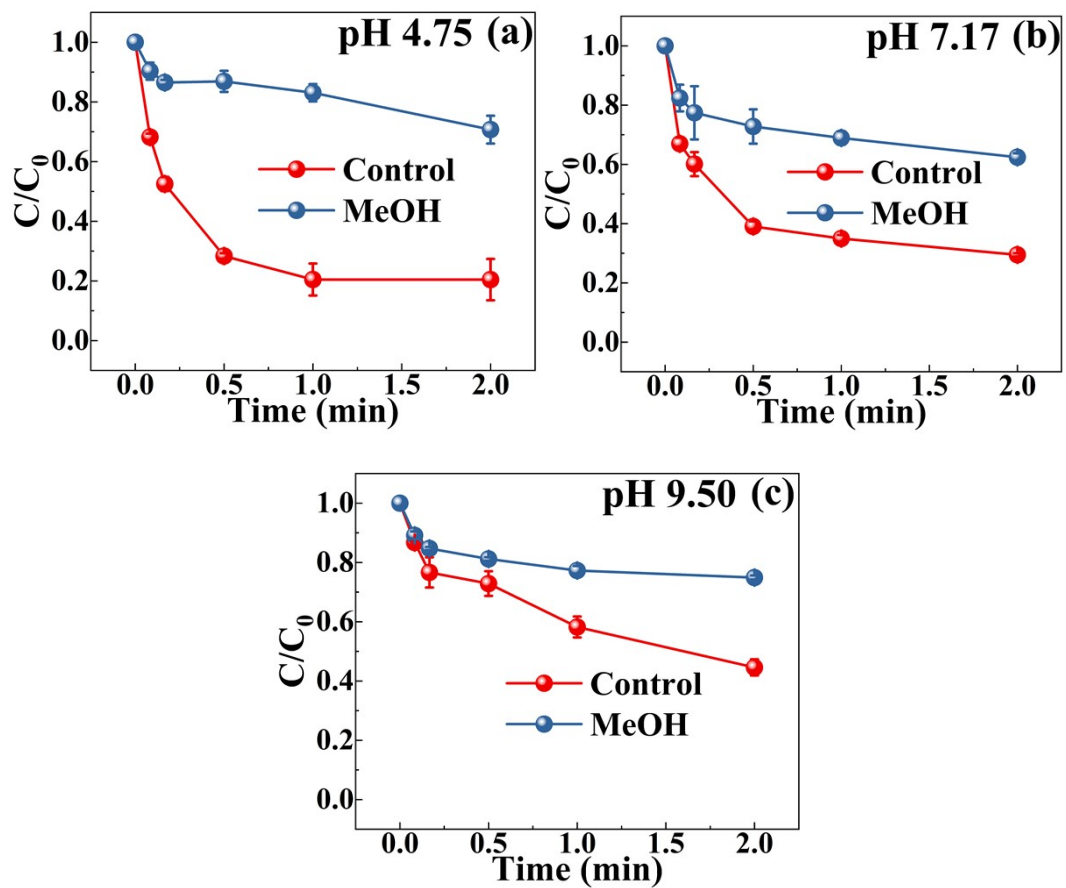[Oxidant]$_0$ = 0.5 mmol/L, [Catalyst]$_0$ = 0.1 g/L, [BPA]$_0$ = 0.1 mmol/L, [PB]$_0$ = 10 mmol/L, pH = 7.17 and T = 278 K.

Fig. S12. Degradation of BPA in different systems (Cu-SA/H$_2$O$_2$, Cu-SA/PDS, Cu-SA/PMS and Fe^{2+}/H$_2$O$_2$).

[Oxidant]$_0$ = 0.5 mmol/L, [Catalyst]$_0$ = 0.1 g/L, [PB]$_0$ = 10 mmol/L, [BPA]$_0$ = 0.1 mmol/L and T = 278 K.
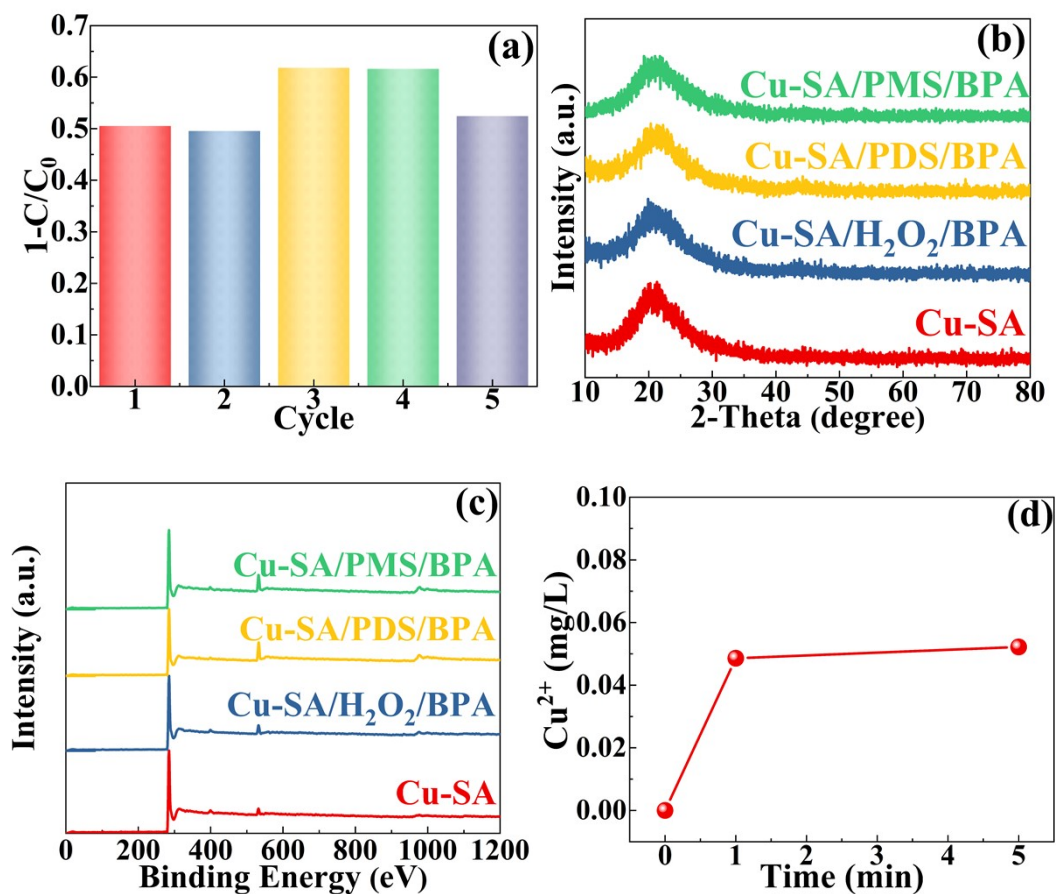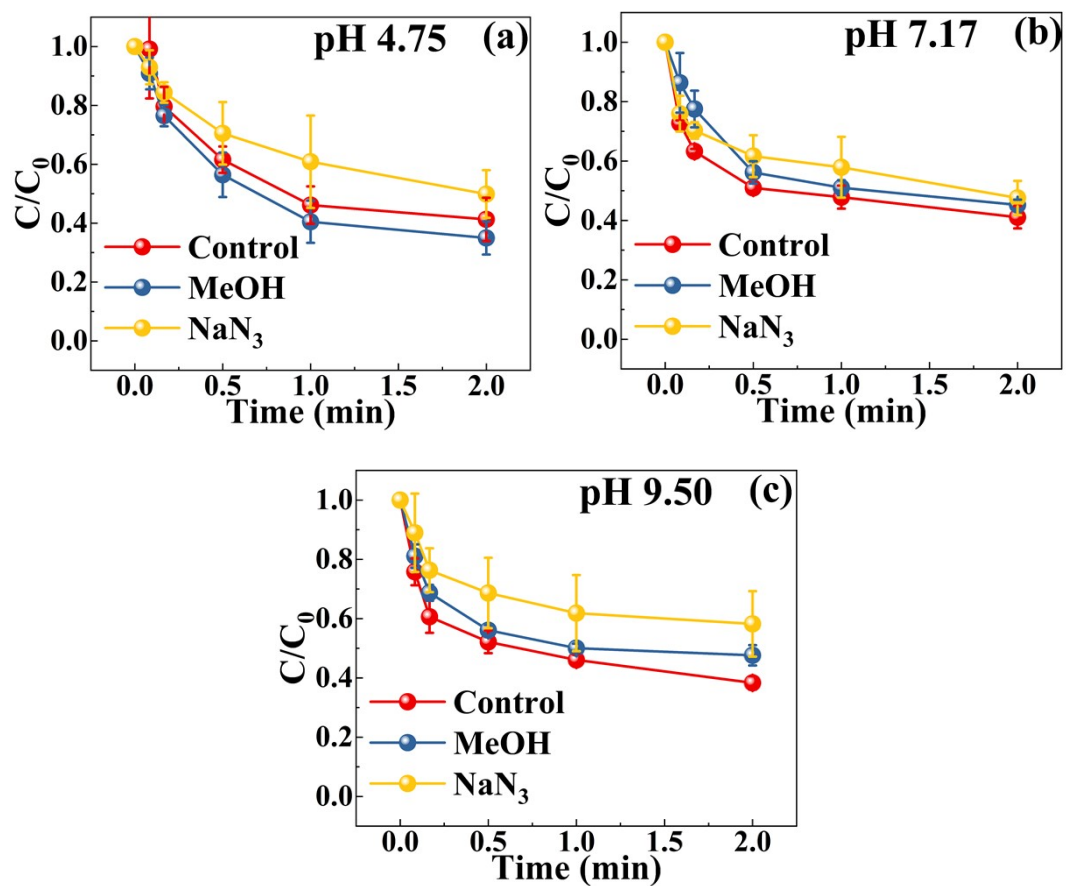
Fig. S13. (a) Cyclic experiment of BPA degradation in Cu-SA/PMS; (b) XRD after Cu-SA reaction; (c) XPS after Cu-SA reaction; (d) Cu^{2+} leaching of Cu-SA.

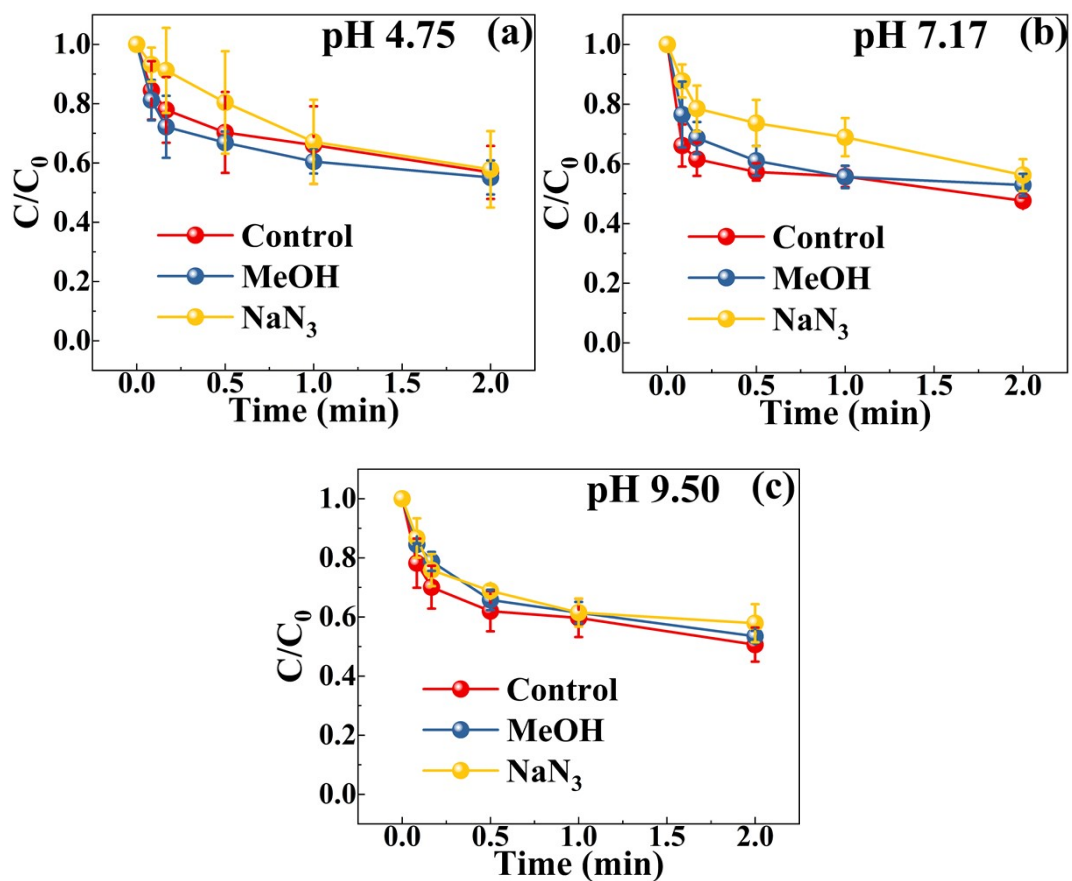$[Oxidant]_0$ = 0.5 mmol/L, $[Catalyst]_0$ = 0.1 g/L, $[BPA]_0$ = 0.1 mmol/L and T = 278 K.

Fig. S14. Influence of MeOH in Cu-SA/H_2O_2.

[Oxidant]$_0$ = 0.5 mmol/L, [Catalyst]$_0$ = 0.1 g/L, [PB]$_0$ = 10 mmol/L [BPA]$_0$ = 0.1 mmol/L and T = 278 K.

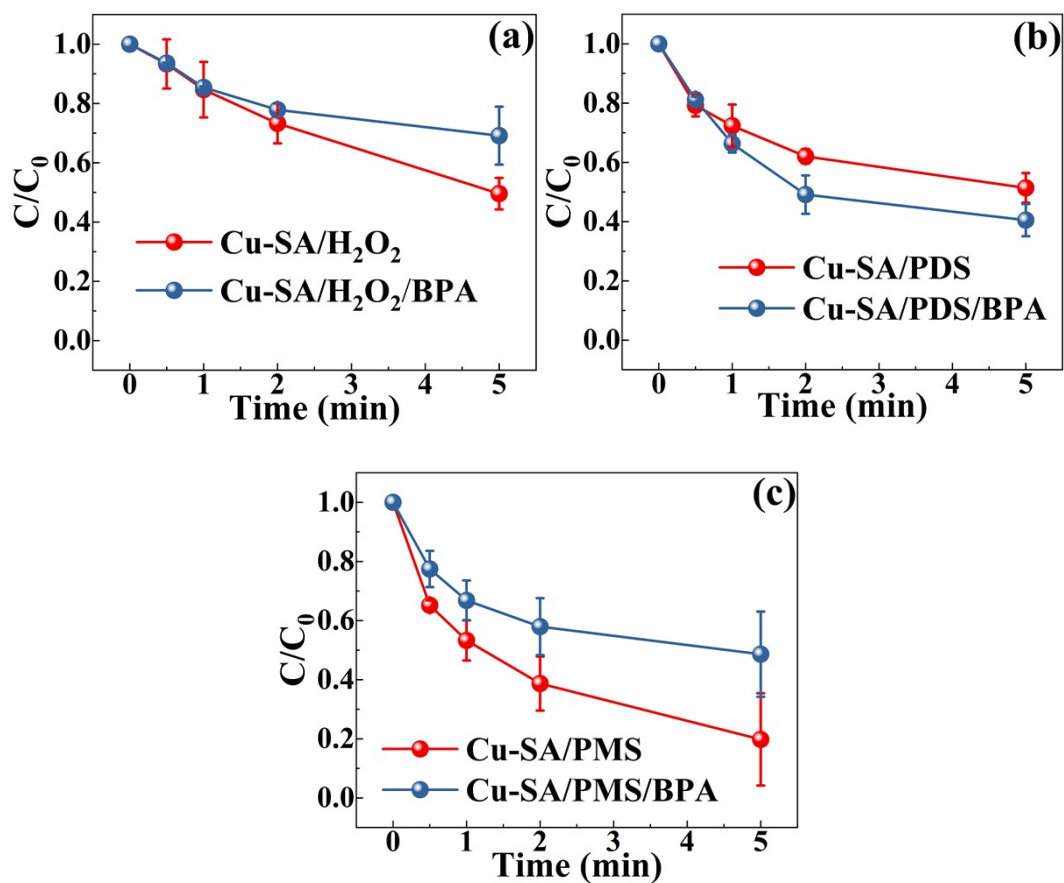**Fig. S15.** Influence of MeOH and NaN$_3$ in Cu-SA/PDS.

[Oxidant]$_0$ = 0.5 mmol/L, [Catalyst]$_0$ = 0.1 g/L, [BPA]$_0$ = 0.1 mmol/L, [PB]$_0$ = 10 mmol/L and T = 278 K.

Fig. S16. Influence of MeOH and NaN$_3$ in Cu-SA/PMS.

[Oxidant]$_0$ = 0.5 mmol/L, [Catalyst]$_0$ = 0.1 g/L, [BPA]$_0$ = 0.1 mmol/L, [PB]$_0$ = 10 mmol/L, [Scavenger]$_0$ = 10 mmol/L and T = 278 K.

Fig. S17. Oxidant consumption in Cu-SA/H$_2$O$_2$, Cu-SA/PDS and Cu-SA/PMS.

[Oxidant]$_0$ = 0.5 mmol/L, [Catalyst]$_0$ = 0.1 g/L, [BPA]$_0$ = 0.1 mmol/L, [PB]$_0$ = 10 mmol/L, pH = 7.17 and T = 278 K.
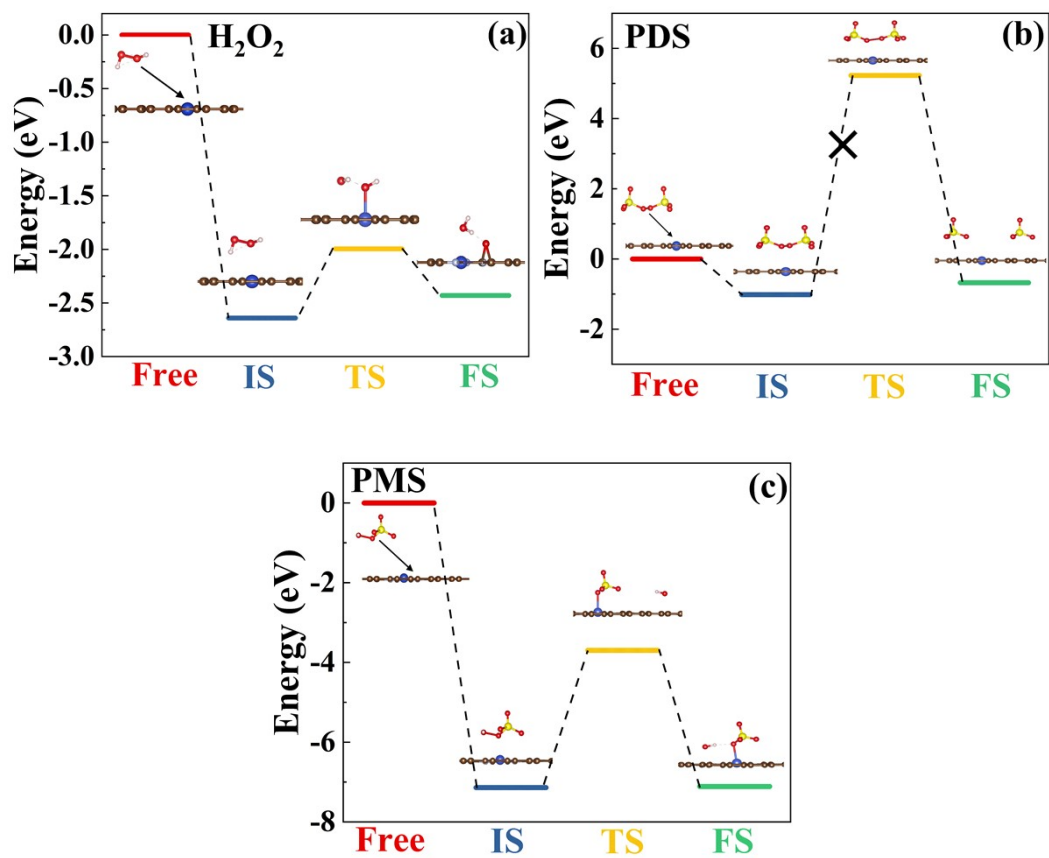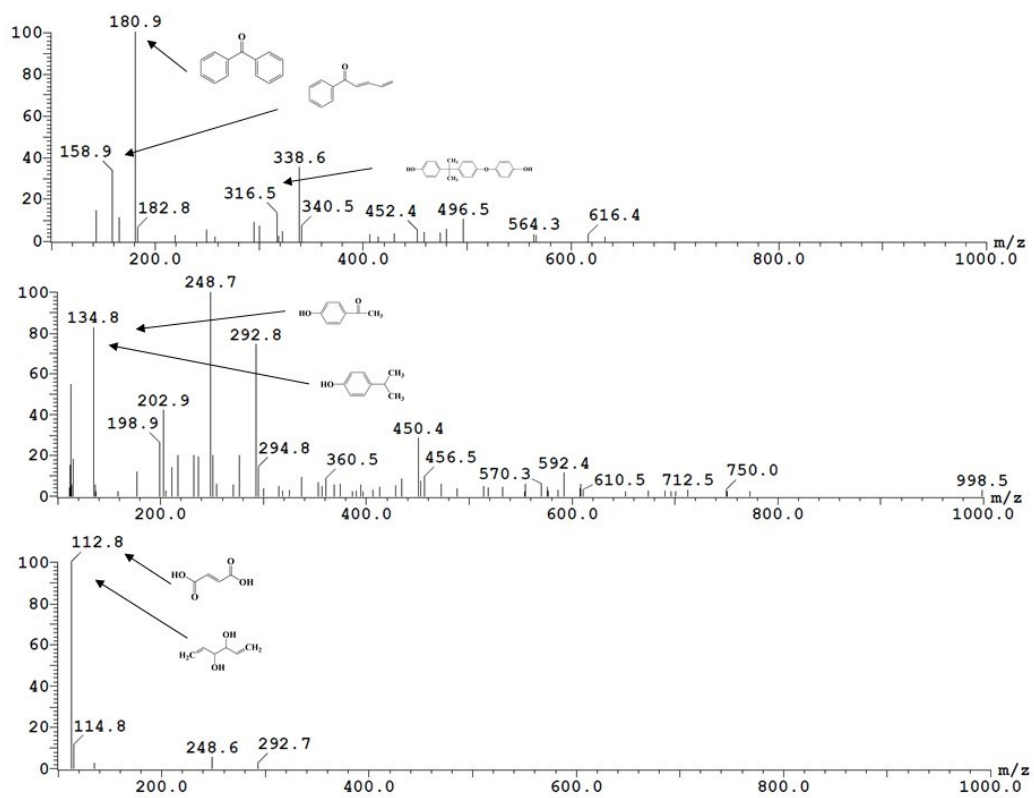
Fig. S18. Minimum energy pathway of (a) H_2O_2, (b) PDS, (c) PMS molecule splitting on surface.

Fig. S19. HPLC-MS of BPA in Cu-SA/H$_2$O$_2$, Cu-SA/PDS and Cu-SA/PMS.

Fig. S20. UV-Vis of BPA in Cu-SA/H_2O_2, Cu-SA/PDS and Cu-SA/PMS.

$[Oxidant]_0$ = 0.5 mmol/L, $[Catalyst]_0$ = 0.1 g/L, $[BPA]_0$ = 0.1 mmol/L, $[PB]_0$ = 10 mmol/L, pH = 7.17 and T = 278 K.
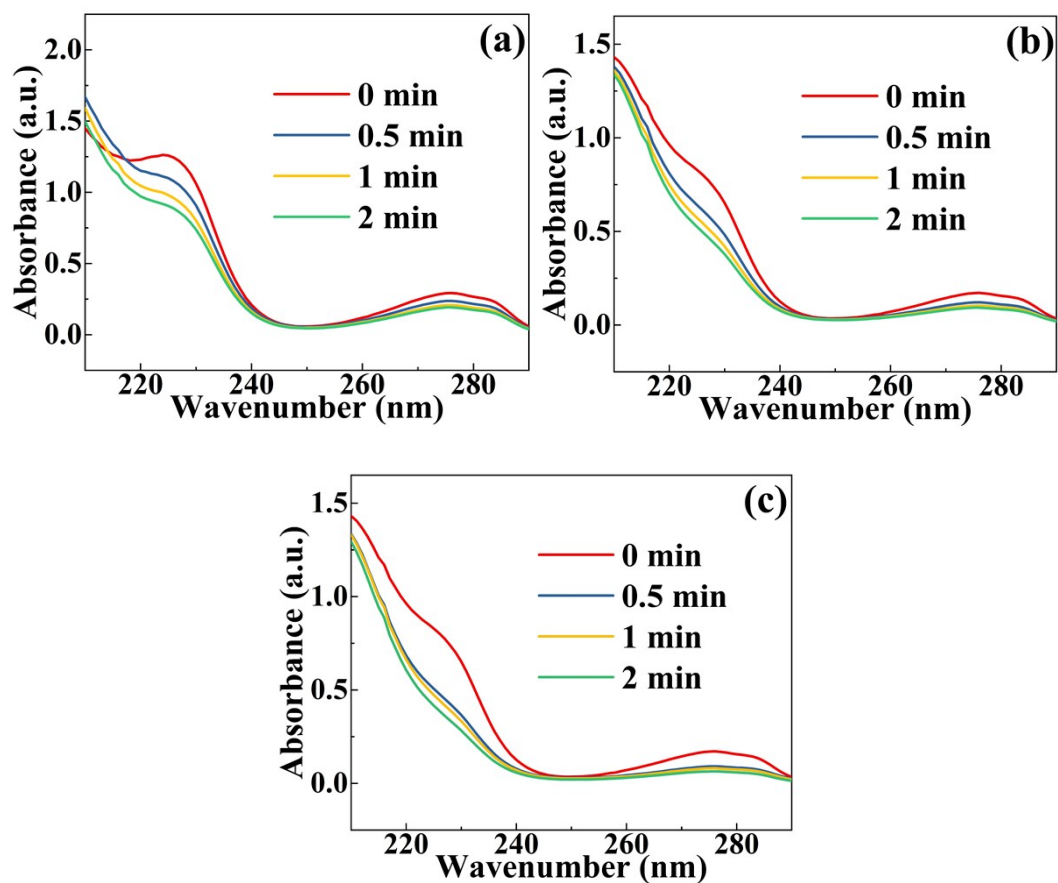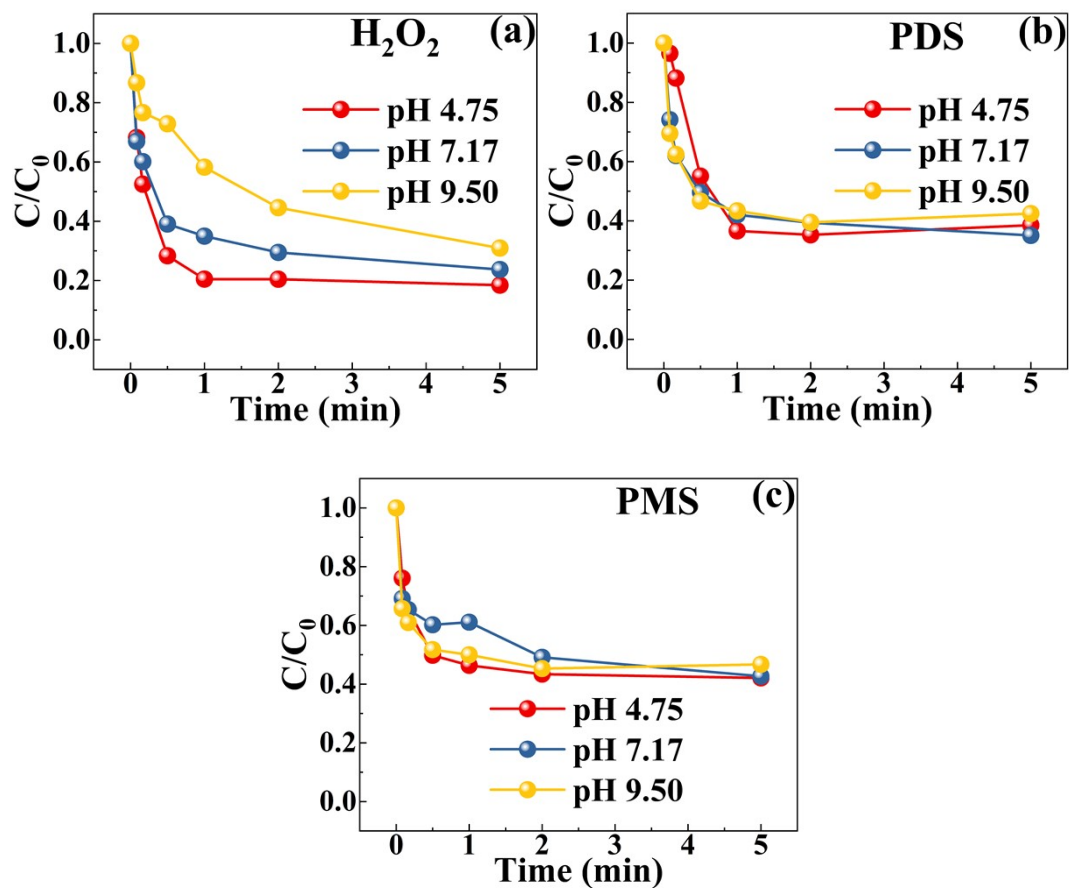
Fig. S21. The effect of pH on the degradation of BPA.

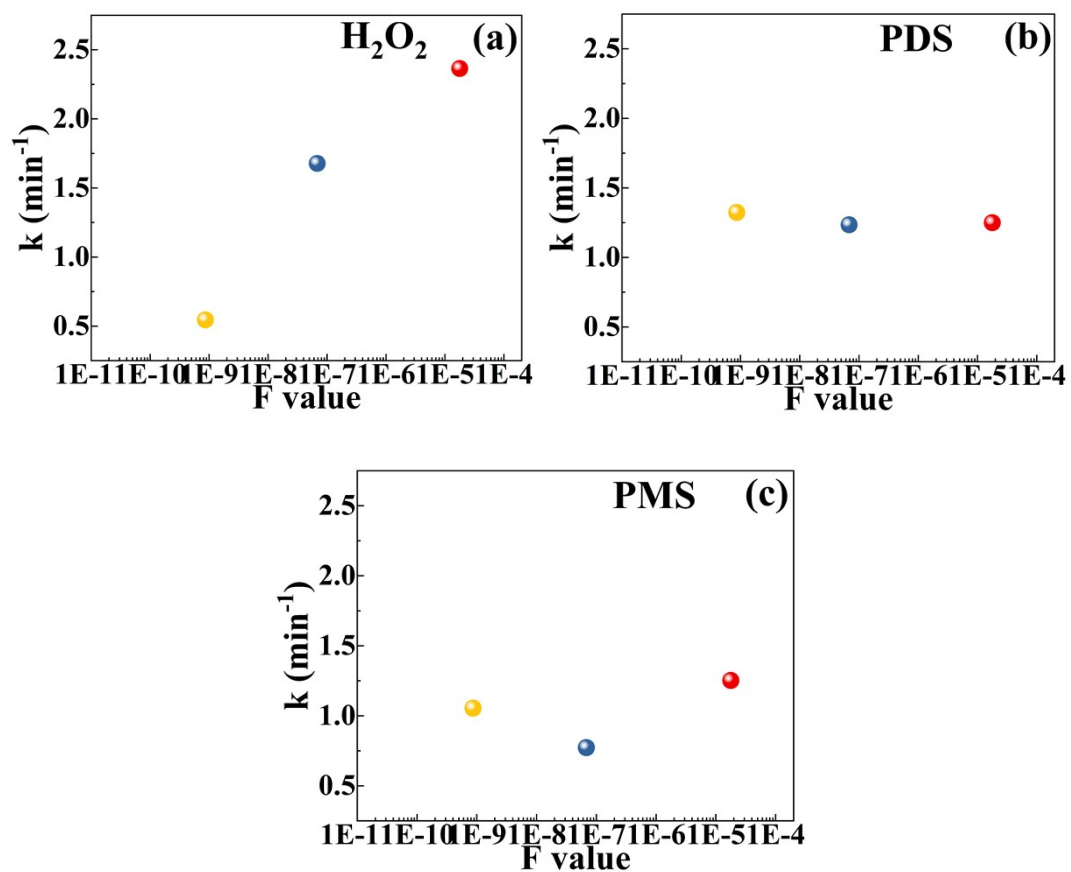[Oxidant]$_0$ = 0.5 mmol/L, [Catalyst]$_0$ = 0.1 g/L, [BPA]$_0$ = 0.1 mmol/L, [PB]$_0$ = 10 mmol/L and T = 278 K.

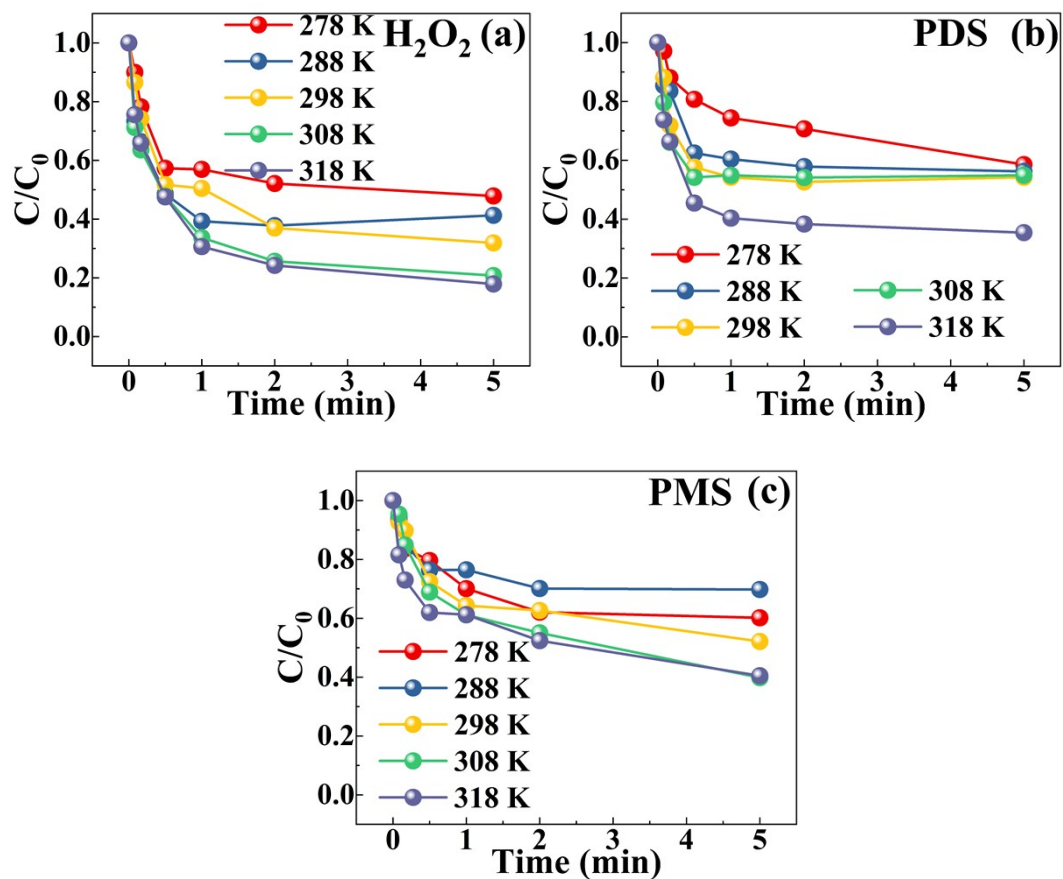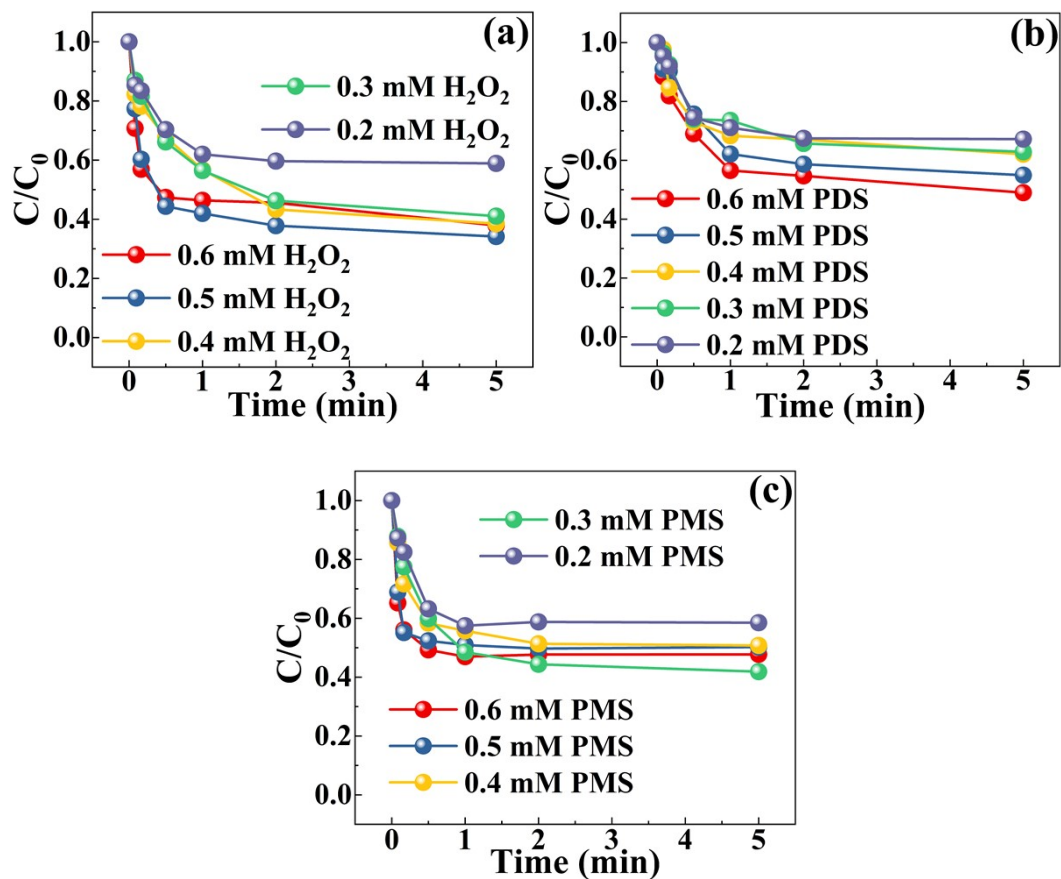**Fig. S22.** The effect of F value.

Fig. S23. The effect of temperature on the degradation of BPA.

[Oxidant]$_0$ = 0.5 mmol/L, [Catalyst]$_0$ = 0.1 g/L, [BPA]$_0$ = 0.1 mmol/L, [PB]$_0$ = 10 mmol/L and pH = 7.17.

Fig. S24. The effect of oxidant concentration on the degradation of BPA.

[Catalyst]$_0$ = 0.1 g/L, [BPA]$_0$ = 0.1 mmol/L, [PB]$_0$ = 10 mmol/L, pH = 7.17 and T = 278 K.
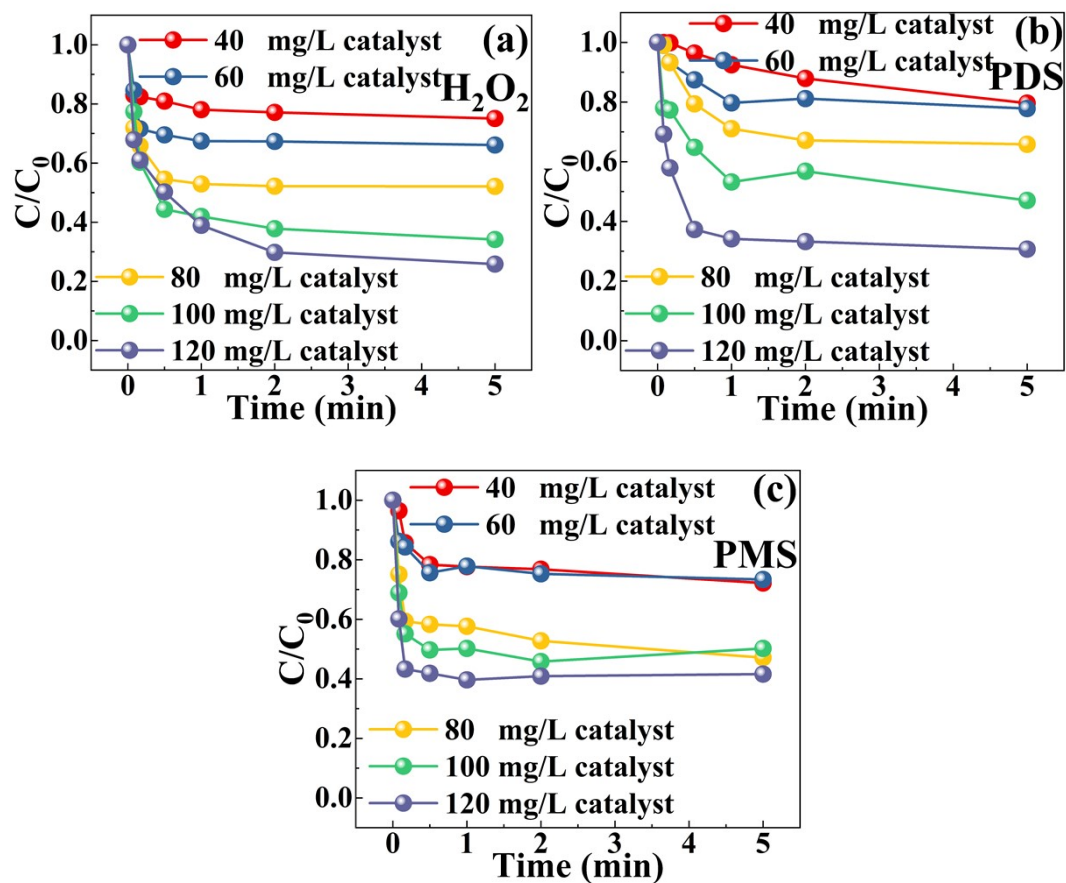
Fig. S25. The effect of catalyst concentration on the degradation of BPA.

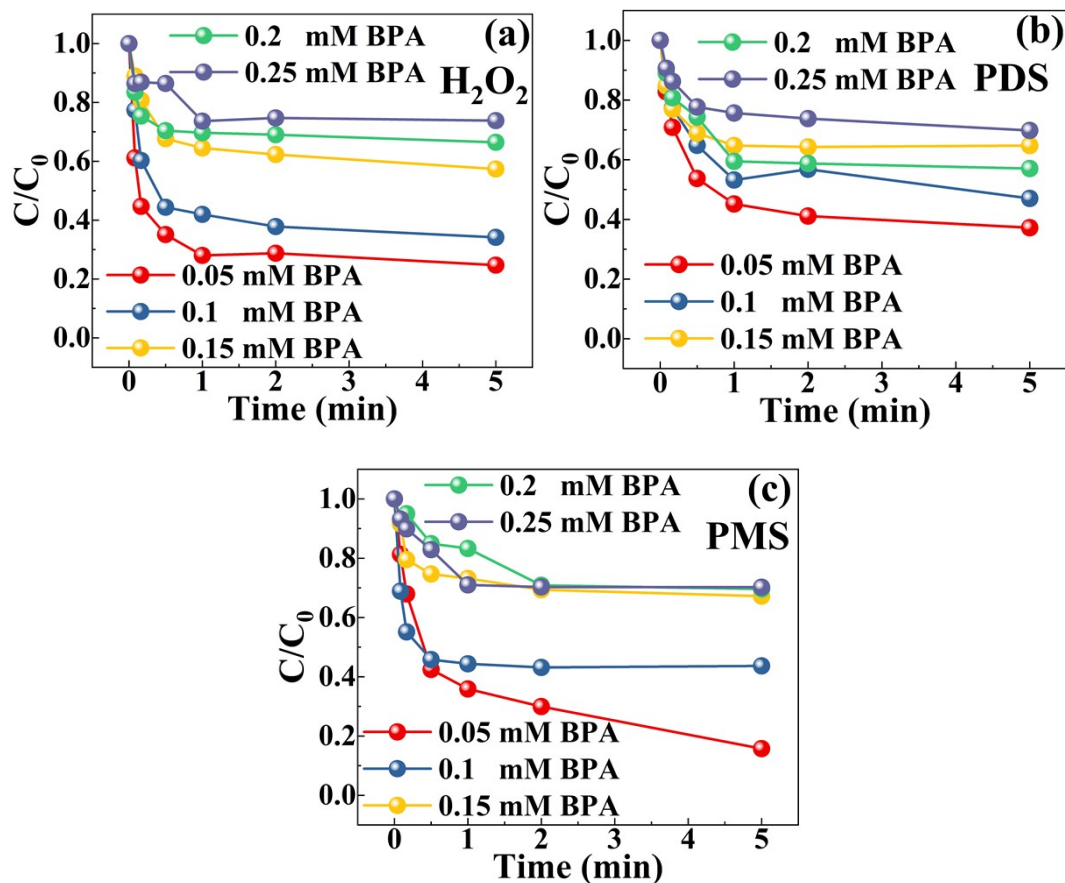[Oxidant]$_0$ = 0.5 mmol/L, [BPA]$_0$ = 0.1 mmol/L, [PB]$_0$ = 10 mmol/L, pH = 7.17 and T = 278 K.

Fig. S26. The effect of BPA concentration on the degradation of BPA.

[Oxidant]$_0$ = 0.5 mmol/L, [Catalyst]$_0$ = 0.1 g/L, [PB]$_0$ = 10 mmol/L, pH = 7.17 and T = 278 K.

Table. S1. The analysis conditions for pollutant.

Contaminant	Flow (ml/min)	λ (nm)	CH$_3$OH	H$_2$O	Remark
Bisphenol A	1.0	280	70	30	HPLC

Table. S2. BET analysis

Sample	Specific surface area (m²/g)	Pore volume (cm³/g)	Average pore size (nm²)
C	992.1534	0.202302 cm³/g	2.26661 nm²
Cu-SA	1,101.9968	0.159822 cm³/g	2.24798 nm²

Table. S3. Best fitting EXAFS data.

Sample	shell	N	R (Å)	σ^2 (10^{-3}Å^2)	R factor
Cu foil	Cu-Cu	12	2.56	8.2	0.003
Cu-SA	Cu-N	4	1.96	5.3	0.007
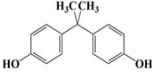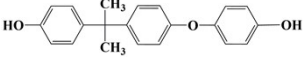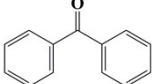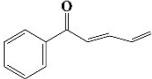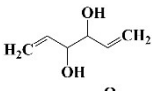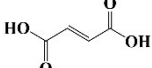
Table. S4. Some comparison of the catalytic performance in similar reported.

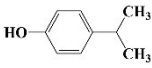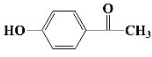| Catalyst	Contaminant	Oxidant	pH	Time (min)	Degradation rate	Ref.
Cu-SA/NGO (0.025 g/L)	Paracetamol (10 mg/L)	H_2O_2 (20 mmol/L)	7.0	60	97.3%	12
SA-Cr/PN-g-C3N4 (0.2 g/L)	Bisphenol A (10 mg/L)	H_2O_2 (163 mmol/L)	7.0	70	98.8%	13
FeCo@NC-1 (0.1 g/L)	Bisphenol A (20 mg/L)	PMS (200 mg/L)	6.0	1	99%	14
0.5UNCu-SBA (0.2 g/L)	p-hydroxybenzoic acid (20 mg/L)	H_2O_2 (1000 mg/L)	4	60	99%	15
Fe-ISAs@CN (0.1 g/L)	Sulfadiazine (2 mg/L)	H_2O_2 (10 mmol/L)	6.5	10	96%	16
Cu-SA (0.1 g/L)	Bisphenol A (0.1 mmol/L)	H_2O_2 (0.5 mmol/L)	7.17	1	81.6%	This work
Cu-SA (0.1 g/L)	Bisphenol A (0.1 mmol/L)	PDS (0.5 mmol/L)	7.17	1	61.5%	This work
Cu-SA (0.1 g/L)	Bisphenol A (0.1 mmol/L)	PMS (0.5 mmol/L)	7.17	1	58.0%	This work

Table. S5. Adsorption energy of H_2O_2, PDS and PMS on Cu-SA.

Sample	E_{ads} (eV)
H_2O_2	-2.64
PDS	-1.02
PMS	-7.14

Table. S6. Intermediate products measured by UPLC-MS.

Number	m/z	Possible intermediates
BPA	228	
P1	317	
P2	181	
P3	158	
P4	135	
P5	135	
P6	113	
P7	113	

References

1.   G. Kresse and J. Furthmüller, *Vienna: Vienna University*, 2001.

2.   W. Kohn and L. J. Sham, *Physical review*, 1965, **140**, A1133.

3.   W. Kohn, A. D. Becke and R. G. Parr, *The Journal of Physical Chemistry*, 1996, **100**, 12974-12980.

4.   P. E. Blöchl, *Physical review B*, 1994, **50**, 17953.

5.   G. Kresse and D. Joubert, *Physical review b*, 1999, **59**, 1758.

6.   J. P. Perdew, K. Burke and M. Ernzerhof, *Physical review letters*, 1996, **77**, 3865.

7.   M. Ernzerhof and G. E. Scuseria, *The Journal of chemical physics*, 1999, **110**, 5029-5036.

8.   S. Grimme, J. Antony, S. Ehrlich and H. Krieg, *The Journal of chemical physics*, 2010, **132**, 154104.

9.   G. Henkelman and H. Jónsson, *Physical review letters*, 2001, **86**, 664.

10.   H. Li, X. Miao, J. Zhang, J. Du, S. Xu, J. Tang and Y. Zhang, *Chemical Engineering Journal*, 2020, **381**, 122680.

11.   R. A. Gaussian09, *Inc., Wallingford CT*, 2009, **121**, 150-166.

12.   Q. Wu, J. Wang, Z. Wang, Y. Xu, Z. Xing, X. Zhang, Y. Guan, G. Liao and X. Li, *Journal of Materials Chemistry A*, 2020, **8**, 13685-13693.

13.   F. Chen, X. L. Wu, C. Shi, H. Lin, J. Chen, Y. Shi, S. Wang and X. Duan, *Advanced Functional Materials*, 2021, **31**, 2007877.

14.   J. Yang, D. Zeng, J. Li, L. Dong, W.-J. Ong and Y. He, *Chemical Engineering Journal*, 2021, **404**, 126376.

15.   Y. Yin, W. Li, C. Xu, L. Shi, L.-C. Zhang, Z. Ao, M. Liu, M. Lu, X. Duan and S. Wang, *Environmental Science: Nano*, 2020, **7**, 2595-2606.

16.   W. Yang, P. Hong, D. Yang, Y. Yang, Z. Wu, C. Xie, J. He, K. Zhang, L. Kong and J. Liu, *Journal of Colloid and Interface Science*, 2021, **597**, 56-65.